

Adsorption of CO on Ni/Cu(110) bimetallic surfacesE. Demirci,¹ C. Carbogno,² A. Groß,² and A. Winkler^{1,*}¹*Institute of Solid State Physics, Graz University of Technology, Petersgasse 16, A-8010 Graz, Austria*²*Institute for Theoretical Chemistry, Ulm University, D-89069 Ulm, Germany*

(Received 14 April 2009; published 17 August 2009)

The adsorption behavior of CO on bimetallic Ni/Cu(110) surfaces has been studied experimentally by thermal-desorption spectroscopy and theoretically by density-functional theory (DFT) calculations. The bimetallic surfaces were produced either by evaporation of nickel or by decomposition of Ni(CO)₄ on Cu(110). Adsorption of CO at 180 K on such a bimetallic surface yields three new adsorption states with adsorption energies between that of CO on clean Cu(110) and clean Ni(110). The new desorption peaks from the bimetallic surface, designated as β_1 - β_3 , can be observed at 250, 300, and 360 K, respectively. These new states are most pronounced when $\frac{1}{2}$ monolayer of nickel is present on the copper surface. DFT calculations, using the Vienna *ab initio* simulation package code, were performed to identify the most probable Ni/Cu atomic arrangements at the bimetallic surface to reconcile with the experimental results. It turned out that CO adsorption on nickel dimers consisting of in-surface and adjacent subsurface atoms can best explain the observed experimental data. The result shows that CO adsorption is determined by local (geometric) effects rather than by long-range (electronic) effects. These findings should contribute to a better understanding of tailoring catalytic processes with the help of bimetallic catalysts.

DOI: [10.1103/PhysRevB.80.085421](https://doi.org/10.1103/PhysRevB.80.085421)

PACS number(s): 68.43.Bc, 68.43.Fg, 68.47.De

I. INTRODUCTION

Bimetallic surfaces play a decisive role in heterogeneous catalysis. Due to the particular arrangement of the different atoms at the surface, new reaction pathways can be opened and both the activity and selectivity of catalysts can be improved. Various concepts for the specific reaction properties of bimetallic surfaces have been discussed in the literature, amongst them the most important are the (electronic) ligand effect and the (geometric) ensemble effect.¹ In recent years this subject has been addressed in several excellent review papers, e.g., by Campbell,² Goodman,³ Rodriguez,⁴ Ponc, ⁵ and Chen *et al.*,⁶ to name just a few. Very recently increased effort has been made to get an improved understanding of the properties of bimetallic surfaces by using theoretical approaches, mainly by using density-functional theory (DFT) calculations.⁶⁻⁹

A very attractive model system of bimetallic surfaces is the Ni/Cu system. These bulk metals have very similar geometric properties. They both crystallize in the face-centered-cubic (fcc) system and their lattice constants are 3.52 Å (Ni) and 3.61 Å (Cu), respectively. On the other hand their electronic and magnetic properties are very different. The non-magnetic noble-metal copper has a filled *d* band and therefore the electron density at the Fermi level is rather small. The magnetic transition-metal nickel has a partially filled *d* band, which leads to a high electron density at the Fermi level. The consequence of this difference is a much higher reactivity of nickel surfaces than that of copper surfaces. However, for the proper activity and selectivity of a particular catalyst often a very distinct surface reactivity is required. A too low reactivity may result in a poor turn over frequency, whereas a too high reactivity of the surface atoms can lead to permanent adsorption of some reaction partners and therefore to poisoning (Sabatier principle¹⁰). This is exactly what makes the bimetallic surfaces so attractive because one can

expect to be able to tune the surface reactivity at will.

In this work we use carbon monoxide as a probe molecule to test the adsorption properties of a Ni/Cu(110) bimetallic surface. It is known that CO desorbs from a Cu(110) surface already at around 210 K,^{11,12} whereas CO is much more strongly adsorbed on Ni(110) and desorbs around 420 K.^{13,14} In an early experiment Yu *et al.*¹⁵ studied already the CO interaction with the surface of a 10% Cu/90% Ni bulk alloy, where the surface composition was varied by heat treatments and sputtering. They came to the conclusion that the CO activation energy of desorption is mainly due to the local molecule-surface arrangement (ensemble effect) but that in addition the CO desorption energy from a Ni site decreases linearly with increased Cu concentration on the surface, indicating that long-range electronic effects (ligand effects) are also present in the bonding. A somewhat later performed theoretical study by Castellani,¹⁶ using a cluster approach and the extended Hückel method to calculate the electron energies, underlined the importance of the ligand effect. In the present work we come to the conclusion that local site effects (ensemble effects) play the major role in CO adsorption and desorption. This assumption is corroborated by DFT calculations.

II. EXPERIMENTAL DETAILS

The experiments were performed in an ultrahigh-vacuum chamber with a base pressure of 1×10^{-10} mbar. The chamber was equipped with an Auger electron spectrometer (AES), a low-energy electron-diffraction (LEED) optics, a quadrupole mass spectrometer, an Ar⁺ ion gun, an electron-beam evaporator, and a quartz microbalance. The Cu(110) single crystal (disk shape, 10 mm in diameter, and 2 mm thickness) was suspended by thin Ta wires inserted in the grooves at the rim of the sample. Controlled heating of the sample was performed via resistive heating. A NiCr-Ni ther-

mocouple was used to control the temperature and regulate a power supply. A heating rate of 2 K/s was typically applied. The sample could be heated up to 1000 K and cooled to 100 K by LN₂ cooling. Sample cleaning was performed by Ar⁺ sputtering at 300 K, followed by annealing at 800 K. After this process a sharp (1 × 1) LEED pattern was observed with no impurities measurable by AES within the detection limit.

For the preparation of the nickel-copper bimetallic surface we applied two different methods. In the first case a nickel covered Cu(110) surface could be prepared by dosing a gas mixture of CO and Ni(CO)₄ at the appropriate surface temperature (180 K). This mixture was unintentionally obtained when CO was filled into a stainless-steel gas inlet system and after a residence time of about 3 month. A semiquantitative calculation yielded a mixture ratio of CO:Ni(CO)₄ ≈ 1000:1 for the gas effusing from the doser. The reason for the synthesis of this gas mixture in the gas line is not quite clear. It is probably related to some catalyzing defects or impurities in the gas inlet system. It is known that nickel carbonyl, which is highly toxic, can easily be formed by CO on nickel surfaces.^{17,18} However, the storage of CO in another stainless-steel gas line did not result in a detectable amount of nickel carbonyl after the same residence time. Nevertheless, we took advantage of this gas mixture to study the concomitant decomposition of nickel carbonyl and the adsorption of CO on the altered Cu(110) surface. This work should also demonstrate that small traces of Ni(CO)₄ in the CO gas phase can cause tremendous (usually unwanted) effects in CO adsorption and desorption studies.

Alternatively, to check the validity of the above-described preparation method, nickel was evaporated onto the Cu(110) surface by a commercial electron-beam evaporator. The amount of evaporated nickel was measured with a quartz microbalance, which could instead be positioned in front of the evaporator. This allowed the quantitative determination of the nickel coverage and hence of the stoichiometry of the bimetallic surface. Combined with Auger electron spectroscopy also the influence of the surface temperature on the formation of the bimetallic layer could be studied. CO adsorption on the such prepared Ni/Cu(110) surface was then performed typically at 130 K.

III. COMPUTATIONAL DETAILS

The aim of the calculations was to identify the various adsorption configurations of CO on the bimetallic surface which lead to the observed discrete desorption peaks. The calculations were performed with the Vienna *ab initio* simulation package (VASP).¹⁹ Electronic exchange and correlation were described in the general gradient approximation, using the functional proposed by Perdew *et al.*²⁰ The wave function is represented by a plane-wave basis set with an energy cutoff of 400 eV. The ion cores were represented by the projector augmented wave method.²¹ A Monkhorst-Pack mesh of 11 × 11 × 1 *k* points was used for the (1 × 1) surface unit cell [5 × 5 × 1 *k* points for the (2 × 2) unit cell] to achieve an accurate description of the density of states near the Fermi level.

The substrate was modeled by slabs typically consisting of five copper layers and one nickel layer with the appropri-

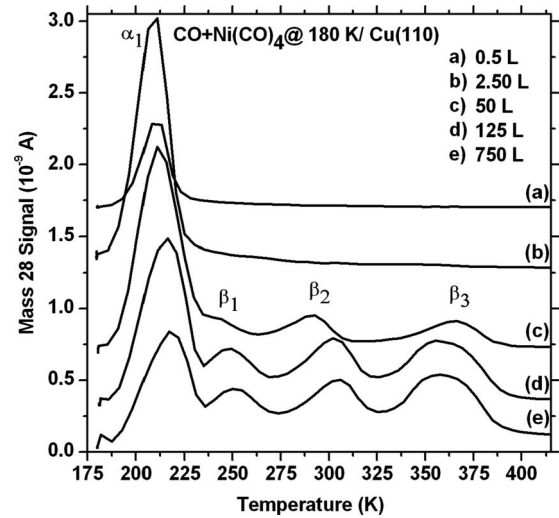


FIG. 1. Set of CO desorption spectra after dosing the initially clean Cu(110) surface with various amounts of the CO+Ni(CO)₄ gas mixture at 180 K. Heating rate: 2 K/s.

ate coverage. The periodicity of the nickel overlayer and of the CO layer was modeled by a (2 × 2) unit cell with 1–4 atoms (molecules) in the basis. The slabs were separated by a 13 Å thick vacuum. The coordinates of the upper two copper layers and the nickel layer, as well as that of the CO molecules, were allowed to relax while the remaining substrate layers were fixed at the bulk position. Geometrical relaxations were carried out using the Hellman-Feynman forces until the energies of the corresponding minima were converged to values with a remaining error below $\Delta E = 0.5$ meV.

IV. EXPERIMENTAL RESULTS

A. CO desorption from Cu(110) after exposure to a CO+Ni(CO)₄ gas mixture

A set of thermal-desorption spectra of CO taken after in-line dosing a Cu(110) surface at 180 K with different exposure of a CO+Ni(CO)₄ gas mixture is shown in Fig. 1. Exposures are given in Langmuir equivalents (1L = 10⁻⁶ Torr s) obtained from the isotropic CO pressure increase and by taking into account an experimentally determined enhancement factor of 5.0 for in-line dosing of CO. Small exposure values (up to about 2.5 L) lead to a rapidly increasing desorption peak at around 210 K, which is due to desorption of CO from the still nearly clean Cu(110) surface.^{11,12} With increasing exposure new desorption peaks start to emerge at around 250, 300, and 360 K. These peaks do not show up when the sample is dosed with the same exposure of pure carbon monoxide. It is obvious that these new peaks have to be correlated with nickel on the surface, resulting from dissociation of nickel tetracarbonyl, as verified by Auger electron spectroscopy. While these new desorption peaks, labeled β_1 (250 K), β_2 (300 K), and β_3 (360 K), increase with increased dosing of the gas mixture, the intensity of the CO desorption peak around 210 K (α_1) goes through a maximum at about 2 L and decreases again for

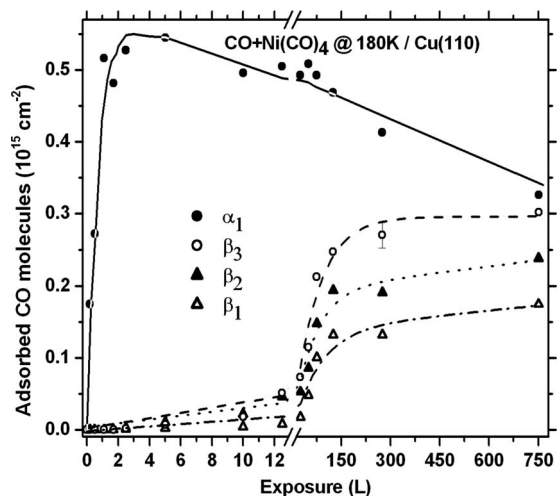


FIG. 2. Uptake curves for CO when dosing the Cu(110) surface with the $\text{CO}+\text{Ni}(\text{CO})_4$ gas mixture, as obtained from a series of TDS, including those in Fig. 1.

higher exposure. In addition to that the desorption peak maxima of the α_1 peak shift by about 10 K to higher temperature. The corresponding uptake curves for the individual desorption peaks are shown in Fig. 2. Above 300 L the β peaks saturate, indicating a saturation of the nickel coverage. From the observed (1×2) LEED pattern and by comparison with the CO desorption spectra after calibrated nickel evaporation (see below) we suppose that the maximum nickel coverage under these experimental conditions corresponds to about $\frac{1}{2}$ monolayer (ML).

Finally, we have exposed the Cu(110) surface to the gas mixture for extended time at 400 K. After a very high exposure (37 000 L) and a subsequent heating to 500 K an Auger analysis showed a clean nickel spectrum, without any detectable Cu signal or signals from other impurities, like carbon. The LEED pattern showed a (1×1) structure. This demonstrates that under these experimental conditions a thick epitaxial nickel film can be grown on the Cu(110) surface by decomposition of nickel carbonyl. The desorption spectrum of CO from this surface was equivalent to literature data for CO desorption from a Ni(110) surface.^{13,14} It is important to emphasize that such a thick nickel layer on Cu(110) remains stable over extended time even at the rather high sample temperature of 500 K. On the other hand, for small nickel coverages, as prepared at 180 K, some of the nickel atoms dissolved in the bulk during heating of the sample to 500 K.

B. CO desorption from a Ni/Cu(110) surface prepared by Ni evaporation

In order to double check the above-described desorption behavior of CO we have performed CO adsorption/desorption experiments on a nickel covered Cu(110) surface prepared by direct evaporation of nickel. The advantage of this procedure is that the amount of evaporated nickel can be determined quantitatively by a quartz microbalance. Furthermore, the sample temperature can be independently adjusted for nickel evaporation and CO adsorption, respectively. In

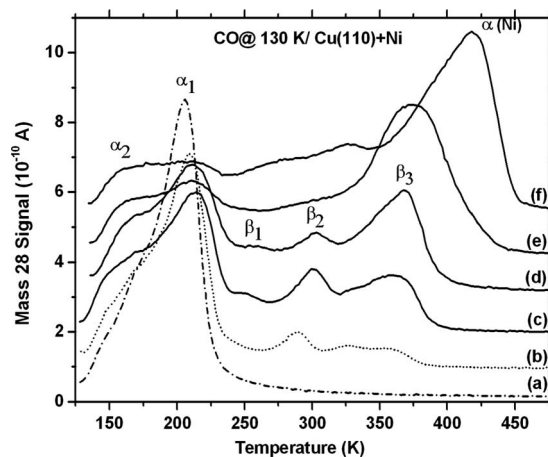


FIG. 3. CO desorption spectra after dosing 3 L CO at 130 K on a Cu(110) surface, covered with various amounts of nickel. Nickel was evaporated onto the surface at 175 K. (a): clean surface, (b): 0.05 ML Ni, (c): 0.19 ML Ni, (d): 0.27 ML Ni, (e): 1.02 ML Ni, and (f): 4.4 ML Ni.

Fig. 3 a series of CO saturation desorption spectra (CO exposure: 3 L) from a Cu(110) surface with increasing amounts of nickel is shown. Nickel was evaporated at 175 K and afterward CO was exposed at 130 K. One can clearly see that on the nickel modified Cu(110) surface the same new adsorption sites β_1 , β_2 , and β_3 evolve as after decomposition of nickel carbonyl. The additional shoulder at around 175 K (α_2 -peak) stems from CO adsorption on the clean Cu sites due to the lower adsorption temperature.¹² Similarly as for the nickel carbonyl decomposition the CO peak from clean copper at 210 K (α_1 peak) decreases with increasing nickel coverage while the new desorption peaks start to increase. The only difference is that the β_1 peak, and to some extent also the β_2 peak, is not so well pronounced than in the case of carbonyl decomposition. The β_3 peak, which is located at around 360 K also increases with increasing nickel coverage but eventually starts to shift to higher temperature (at $\Theta_{\text{Ni}} > 1$ ML) with a final peak maximum at 420 K. This is close to the desorption temperature of CO from a pure nickel surface [designated as $\alpha(\text{Ni})$ peak].^{13,14} For this high nickel coverage the original β peaks are rarely visible, indicating that these peaks are related to the bimetallic surface. It should be noted that after each desorption run the surface had to be prepared again, because some of the adsorbed nickel dissolves in the bulk during heating up to 500 K, similarly as in the case of nickel carbonyl decomposition.

Further insight into the effect of adsorbed nickel on CO adsorption can be gained by preparing the nickel layer at different substrate temperatures. In Fig. 4 the change in the relative coverage corresponding to the individual desorption peaks, as a function of the preparation temperature, is compiled. In this case first always 0.2 ML of Ni were evaporated at different temperatures and subsequently 3 L of CO were dosed at 130 K. It is clear that those peaks which are correlated with the bimetallic surface (β_1 - β_3) decrease with increasing preparation temperature, whereas the desorption peaks from the clean Cu surface (α_1 , α_2) increase. This is due to the partial subsurface penetration and subsequent dis-

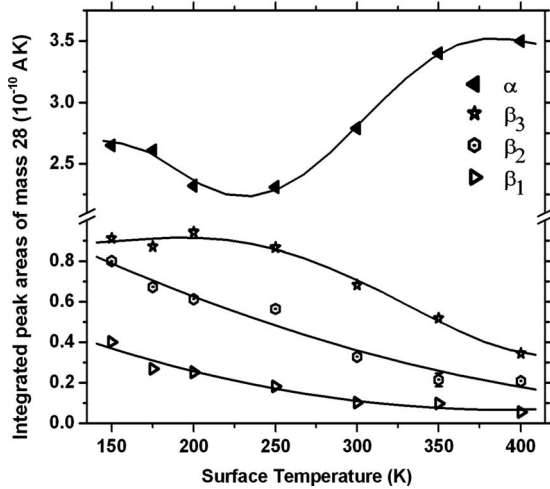


FIG. 4. Change in the amount of adsorbed CO in the individual adsorption sites after preparing the Ni/Cu(110) bimetallic surface by evaporation of 0.2 ML nickel at different substrate temperatures. Subsequent CO exposure at 130 K is 3 L.

solution of nickel in the copper bulk at elevated temperature.

One additional experimental feature should be mentioned in this context. A comparison of the CO desorption spectra as obtained after decomposition of nickel carbonyl with that obtained after adsorption of CO on a Ni covered Cu(110) surface showed that the β peaks are always less pronounced in the latter case. However, if nickel was evaporated onto a CO presaturated Cu(110) surface or if nickel was evaporated in CO atmosphere (1×10^{-8} Torr) then the desorption spectra were very similar to that obtained after nickel carbonyl decomposition.

Finally, in Fig. 5 saturation CO desorption spectra are compared as obtained (a) from the clean Cu(110) surface, (b)

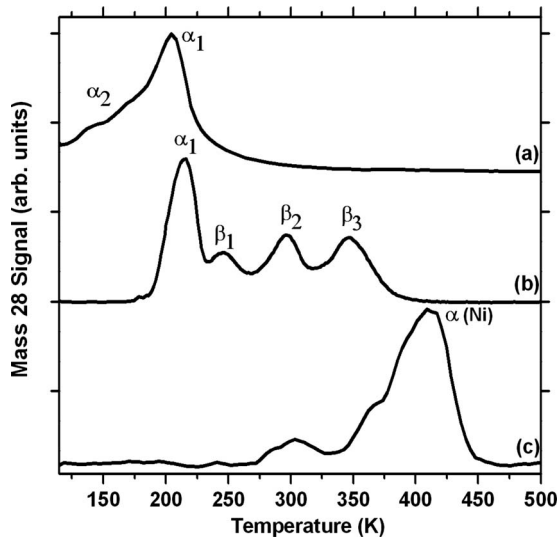


FIG. 5. Compilation of saturation CO desorption spectra after dosing (a) 3 L of pure CO on the clean Cu(110) surface ($T_{\text{ad}} = 110$ K), (b) 250 L of the CO+Ni(CO)₄ gas mixture on the Cu(110) surface ($T_{\text{ad}} = 180$ K), and (c) 3 L pure CO on the epitaxially grown Ni(110) surface ($T_{\text{ad}} = 110$ K).

from the Ni/Cu(110) bimetallic surface as prepared by Ni(CO)₄ decomposition, and (c) from a thick epitaxial Ni(110) film. This compilation shows impressively the potential of the bimetallic Ni-Cu surface to tailor the CO adsorption energy. However, rather than leading to a continuous shift of the adsorption energy for CO on the copper surface with increasing nickel concentration, three new discrete adsorption sites are generated. The origin of these peaks will be clarified by DFT calculations.

V. RESULTS OF THE CALCULATIONS

Before we present the DFT calculations for the adsorption energies and adsorption configurations of CO on the bimetallic Ni/Cu(110) surface we will give a summary of our calculations for CO adsorption on the clean Cu(110) and Ni(110) surfaces. For these systems comprehensive experimental data are available for comparison with the calculations. We would like to point out that we are well aware of the fact that DFT calculations generally yield too high adsorption energies for CO on metal surfaces due to the underestimation of the highest occupied molecular orbital and lowest unoccupied molecular orbital gap of the CO molecule.²² For the (111) planes of fcc metals in some cases even the adsorption sites for CO cannot be calculated correctly.²³ However, for the Cu(110) plane these restrictions seem not to hold.^{24,25} As we will show below a quite good agreement between the calculations and the experimental data with respect to the adsorption configuration is obtained. Concerning the adsorption energies it should at least be possible to calculate the relative trends in the activity of bimetallic systems.⁹

The adsorption energies for CO molecules are determined by using a (2×2) unit cell with $n=1-4$ molecules in the basis to simulate coverages of 0.25, 0.5, 0.75, and 1.0 MLs, respectively. The adsorption energy of the n th molecule is determined by

$$E_{\text{ads}}^{\text{nth}} = E^{n\text{CO}/\text{Cu}} - (E^{(n-1)\text{CO}/\text{Cu}} + E^{\text{CO}}), \quad (1)$$

where $E^{n\text{CO}/\text{Cu}}$ is the total slab energy of the substrate with n adsorbed CO molecules, $E^{(n-1)\text{CO}/\text{Cu}}$ the corresponding total slab energy for $(n-1)$ adsorbed CO molecules, and E^{CO} the total energy of the free CO molecules. It should be noted that the adsorption energy is negative in case of stable adsorption. In this text, however, we use the expressions adsorption energy, desorption energy, and binding energy of CO to the surface synonymously and use the absolute value of the calculated adsorption energy.

A. CO on Cu(110)

From experiments it is known that the maximum coverage of CO on Cu(110), at an adsorption temperature of 110 K, is 0.8 ML. 0.3 ML desorb at ca. 175 K and 0.5 ML at ca. 210 K.¹² For coverages $\Theta_{\text{CO}} \leq 0.5$ ML the adsorption energy was determined to be $0.6 \text{ eV} \pm 10\%$ (Refs. 11, 12, 26, and 27) and only weakly coverage dependent. The LEED pattern of the 0.5 ML covered surface exhibits a weak (2×1) superstructure.^{11,28} This information was taken as a basis for

TABLE I. Tilt angles in the x direction and adsorption energies of CO on Cu(110) as a function of the coverage for given adsorption sites. Compare with Fig. 6.

Coverage (ML)	Tilt angle in the x direction ($^\circ$) n th molecule/C-O/Me-C		Adsorption energy (eV) /(n th molecule)	
0.75(longbridge)	First	35	35	0.46 (first)
	Second	0	0	
	Third	-7	-7	
0.75 (on top)	First	0	0	0.20 (first)
	Second	0	0	
	Third	0	0	
0.50	Second	0	0	0.82(second)
	Third	0	0	
0.25	Third	0	0	0.94 (third)

the modeling. The adsorption energies and adsorption configurations were calculated for different scenarios. In the first scenario two CO molecules (second and third molecules) in the surface unit cell were initially located on top and another molecule (first molecule) at a long bridge site. (The molecules in the surface unit cell are numbered according to their removal from the surface for the energy calculations.) It should be noted that always several calculations were performed with different initial molecule configurations to test the reliability of the calculations for the relaxed final configuration. In Table I the final CO adsorption configuration (tilt angles between C-O and Me-C in the x direction) and the adsorption energies for three different coverage regimes are compiled. Tilting into the y direction is generally small. The molecule configuration for 0.75 ML CO is shown in Fig. 6. We estimate the numerical uncertainty of the calculated energy values to be about ± 20 meV and the uncertainty of the calculated tilt angles to be about $\pm 3^\circ$, depending on the corrugation of the potential. It turns out that the second and third molecules in the surface unit cell remain located at the on-top position after relaxation. These molecules are nearly vertically oriented. (Calculated values of tilt angles below 3°

have been considered as corresponding to vertical orientation.) This result is in good agreement with photoelectron diffraction experiments²⁹ and with other DFT calculations.^{24,25} The adsorption energy for the molecules with $\Theta \leq 0.5$ ML is about 0.9 eV. However, the first molecule in the unit cell (total coverage 0.75 ML) rearranges after relaxation and becomes strongly tilted. The binding energy for these molecules is 0.46 eV. It can be considered as being nearly vertically adsorbed with respect to the (111) facet of the (110) plane in a threefold hollow site and therefore strongly tilted with respect to the surface normal. When the first CO molecule is initially positioned at an on-top site it remains at this site according to the DFT calculations, apparently due to a local potential minimum, but this configuration is energetically much less favorable ($E_{\text{ads}}=0.2$ eV) (see Table I).

We have also calculated the adsorption energies and configurations for the second and third CO molecules in short-bridge positions and it turned out that the adsorption energies are nearly the same as for the on-top configuration (0.9 eV). This shows that only a very weak lateral corrugation of the adsorption well exists along the $[1-10]$ direction and that therefore no pronounced superstructure of the CO overlayer forms on the surface. This also explains why the experimentally obtained LEED patterns of the (2×1) superstructure are generally very weak.^{11,26}

B. CO on Ni(110)

For CO on Ni(110) a saturation coverage of 1 ML at $T_{\text{ads}} < 250$ K has been determined experimentally.¹⁴ The desorption energy remains nearly constant over the whole coverage range and the following values for the adsorption energy can be found in the literature: 1.4,¹³ 1.2,³⁰ and 1.0 eV.¹⁴ For coverages above 0.75 ML a tilting of the CO molecules by about 19° was determined by electron stimulated desorption ion angular distribution (ESDIAD) measurements.³⁰ For our calculations we used again a (2×2) unit cell with 1–4 CO molecules in the basis. The results are compiled in Table II for CO molecules located at on-top sites and short-bridge sites, respectively. For both configurations we obtain tilt angles which are close to the experimentally obtained 19° for

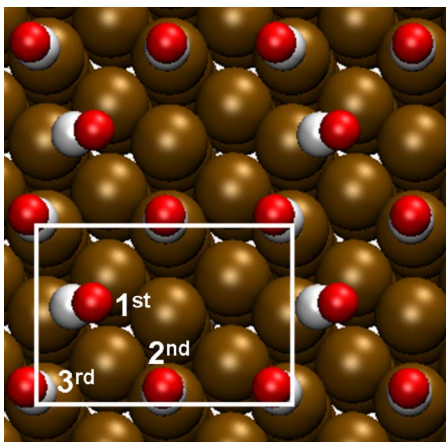


FIG. 6. (Color online) Relaxed CO molecule configuration on a Cu(110) surface for a coverage of 0.75 ML. A (2×2) surface unit cell was used for the calculations and the molecules in the basis of the unit cell are numbered according to their sequential removal.

TABLE II. (a) Tilt angles and adsorption energies of CO on Ni(110) as a function of coverage for molecules in on-top position. (b) Tilt angles and adsorption energies of CO on Ni(110) as a function of coverage for molecules in short-bridge position. Compare with Fig. 7.

	Coverage (ML)		Tilt angle in the x direction ($^{\circ}$) n th molecule/C-O/Me-C		Adsorption energy (eV) /(n th molecule)	
(a)	1	First	-16	-19	1.02 (first)	
		Second	-16	-19		
		Third	16	19		
		Fourth	16	19		
	0.75	Second	-15	-17	1.07(second)	
		Third	-6	-6		
		Fourth	18	17		
	0.50	Third	0	0	1.68 (third)	
		Fourth	0	0		
	0.25	Fourth	0	0	1.70 (fourth)	
	(b)	1	First	-20	-20	1.61 (first)
			Second	-20	-20	
Third			20	20		
Fourth			20	20		
0.75		Second	-15	-16	1.59(second)	
		Third	-5	-5		
		Fourth	17	18		
0.50		Third	0	0	1.77 (third)	
		Fourth	0	0		
0.25		Fourth	0	0	1.83 (fourth)	

$\Theta > 0.5$ ML. However, for the on-top configuration the adsorption energy for coverages $\Theta > 0.5$ ML ($E_{\text{ads}} \approx 1.0$ eV) is significantly different from that for $\Theta < 0.5$ ML ($E_{\text{ads}} \approx 1.7$ eV). On the other hand, when the molecules are located at short-bridge sites the adsorption energies change only from 1.6 eV at $\Theta = 1.0$ ML to 1.8 eV at $\Theta = 0.25$ ML. This is in good agreement with the experimentally obtained small coverage dependence of the adsorption energy. Thus we conclude that the short-bridge configuration is the correct one, at least for high CO coverages, as shown in Fig. 7. This agrees very well to existing ESDIAD (Ref. 30) and electron-energy-loss spectroscopy measurements.³¹

C. CO on bimetallic Ni/Cu(110) surfaces

From our experiments with the dissociation of $\text{Ni}(\text{CO})_4$ on Cu(110) at 180 K we obtain a transient nickel saturation coverage of about $\frac{1}{2}$ ML. This is consistent with the observed LEED pattern of a (1×2) superstructure. By direct nickel evaporation one can, of course, adjust any coverage and in addition also vary the surface temperature. But also in this case the new desorption peaks β_1 - β_3 are most pronounced at a nickel coverage of about 0.5 ML. Thus we have focused our calculations mainly on the bimetallic Ni/Cu(110) surface containing 0.5 ML nickel. Furthermore, we know that the Ni atoms not necessarily remain adsorbed on the surface but that with increasing surface temperature the Ni atoms start to

move into surface and subsurface sites of the copper substrate. This has also been demonstrated by using other experimental techniques, such as HREELS (high-resolution electron-energy-loss spectroscopy),^{32,33} and theoretically by the first-principles Greens's function technique.³⁴ The kinetics of subsurface penetration and finally the dissolution into the bulk, however, depends not only on the temperature but also on the amount of nickel and on the amount of CO ad-

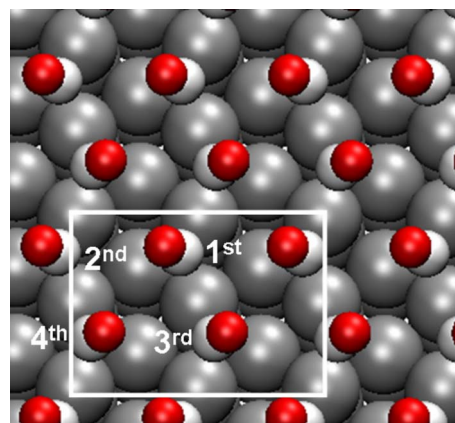


FIG. 7. (Color online) Relaxed CO molecule configuration on a Ni(110) surface for a coverage of 1.0 ML. A (2×2) surface unit cell was used for the calculations and the molecules in the basis of the unit cell are numbered according to their sequential removal.

TABLE III. Tilt angles and adsorption energies of CO on a Ni/Cu(110) bimetallic surface [1/2 ML Ni adsorbed on Cu(110)] as a function of CO coverage. Compare with Fig. 8.

Coverage (ML)		Tilt angle in the x direction ($^{\circ}$) n th molecule/C-O/Me-C		Adsorption energy (eV) /(n th molecule)
1	First	-48	-12	0.50 (first)
	Second	46	10	
	Third	17	7	
	Fourth	21	-10	
0.75	Second	42	-9	0.84(second)
	Third	-39	-44	
	Fourth	-12	-10	
0.50	Third	-26	-25	1.94 (third)
	Fourth	26	25	
0.25	Fourth	0	0	2.21 (fourth)

sorbed on the surface, as will be outlined in the discussion.

Our own DFT calculations also yield an increase in the (negative) total energy of the Ni/Cu(110) system when moving the Ni atoms from the adsorbed sites into the in-surface sites (surface alloy) and further into the subsurface sites. However, when CO molecules were adsorbed on the Ni covered Cu(110) surface, the Ni atoms tend to remain at the surface (see below).

We have therefore performed our calculations of CO adsorption on the Ni-Cu bimetallic surfaces for different scenarios: (a) $\frac{1}{2}$ ML Ni adsorbed on the Cu(110) surface in fourfold hollow sites in a (1×2) superstructure, (b) A 1:1 Ni-Cu surface alloy with alternating rows of Ni and Cu in $[1-10]$ direction, (c) $\frac{1}{2}$ ML subsurface Ni in fourfold hollow sites in a (1×2) superstructure configuration, (d) $\frac{1}{2}$ ML Ni forming a mixture of adsorbed and in-surface sites along the $[1-10]$ direction, and (e) $\frac{1}{2}$ ML Ni forming a mixture of in-surface and subsurface nickel on Cu(110), the calculated values for the adsorption energies can be best reconciled with the experimental data.

1. CO on $\frac{1}{2}$ ML Ni adsorbed on Cu(110) in a (1×2) superstructure

Again we have used a (2×2) supercell with 1–4 CO molecules in the basis and have started with various initial CO configurations to find the most favorable final constellation of the molecules after relaxation. The values for the adsorption energies and the tilt angles are compiled in Table III and the ball models for the arrangement of the CO molecules on the bimetallic surface for different coverages are depicted in Figs. 8(a)–8(d). For all scenarios the common feature is that the CO molecules are always attracted to the Ni atoms. In the case of 1 ML coverage half of the molecules are located in Ni short-bridge positions and they are slightly tilted (third and fourth molecules). The second half (first and second molecules) are located in threefold hollow sites of the (111) facets of the (110) surface and these molecules are strongly tilted [Fig. 8(a)].

It is remarkable that due to the strong interaction with the CO molecules the Ni atoms are laterally displaced and they form a zigzag row along the $[1-10]$ direction. The alternating displacement is $+0.25$ and -0.30 Å, respectively. The removal of one CO molecule from the unit cell (first CO), which costs an energy of 0.5 eV, leads to a further striking redistribution of the remaining CO molecules ($3/4$ ML total coverage). A quite symmetric situation is established where every second short-bridge site is occupied by nearly vertical CO molecules and in between two CO molecules occupy threefold hollow sites of the (111) facets and are therefore strongly tilted [Fig. 8(b)]. The lateral displacement of the Ni atoms is lifted. The desorption energy for the next (second) CO molecule is 0.84 eV and the configuration of the remaining CO molecules changes again ($1/2$ ML total coverage). The CO molecules are now arranged in short-bridge sites of the Ni rows alternately tilted by about 26° . Figure 8(c) shows a side view of this configuration. This

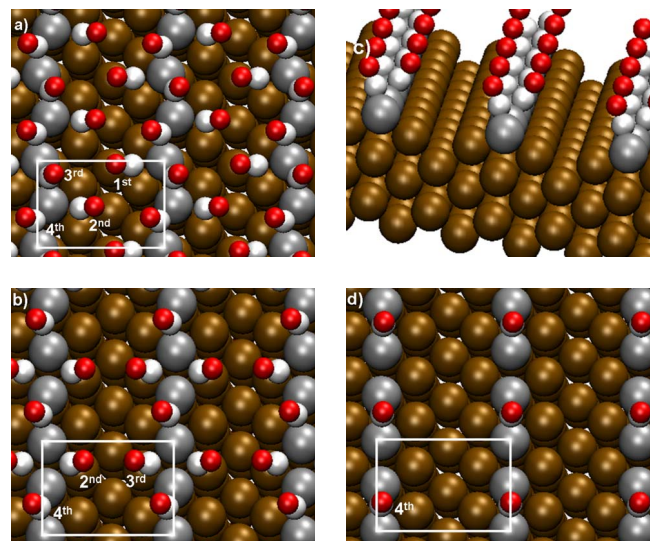


FIG. 8. (Color online) [(a)–(d)]: Relaxed CO molecule configuration on a Ni/Cu(110) bimetallic surface with $\frac{1}{2}$ ML nickel adsorbed in a (1×2) superstructure. (a) 1.0 ML CO, (b) 0.75 ML CO, (c) 0.5 ML CO, and (d) 0.25 ML CO.

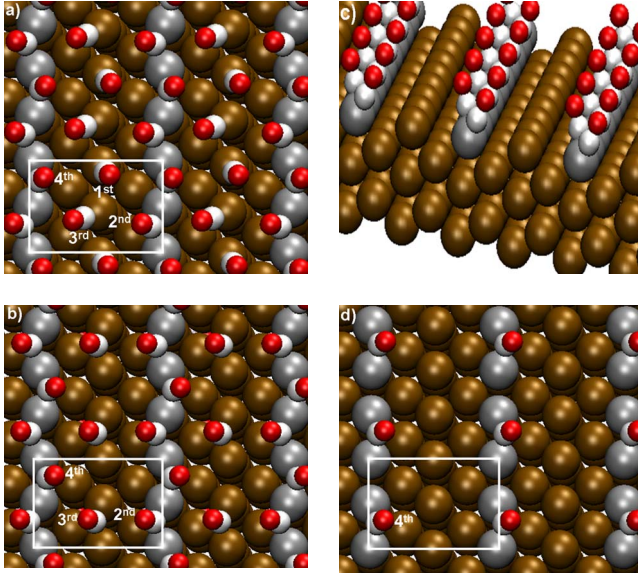


FIG. 9. (Color online) [(a)–(d)]: Relaxed CO molecule configuration on a 1:1 Ni/Cu surface alloy (a) 1.0 ML CO, (b) 0.75 ML CO, (c) 0.5 ML CO, and (d) 0.25 ML CO.

situation is similar to the 1 ML coverage on the clean Ni(110) surface. Removing the next CO molecule from the unit cell (third CO molecule), which costs an energy of 1.94 eV, leads to a situation where on every second short-bridge site of the Ni rows a CO molecule is adsorbed in a vertical arrangement [$1/4$ ML coverage, Fig. 8(d)]. The desorption energy for these last molecules is 2.21 eV.

2. CO adsorption on a 1:1 Ni/Cu surface alloy

The adsorption behavior of CO on the Ni-Cu surface alloy clearly differs from that in the previous case. The adsorption configurations for various CO coverages are shown in Figs. 9(a)–9(d) and the tilt angles and adsorption energies are compiled in Table IV. In case of the 1 ML coverage less CO molecules can be adapted at the Ni rows. Half of the CO molecules are bonded to Ni atoms at short-bridge sites and they are alternately tilted. The other half of the molecules

occupy on-top Cu sites and they are also tilted [Fig. 9(a)]. The latter molecules are much weaker bound and can be removed first. After removal of the first molecule (adsorption energy 0.38 eV) the molecules bound to the Ni atoms are only little effected. However, the on-top copper bound CO molecules shift to short-bridge positions. The removal of these (second) molecules costs 0.82 eV. For desorption of the remaining, nickel bonded, molecules a much higher energy is needed. The adsorption energy of the third CO molecule is 1.73 eV and of the fourth molecule it is 2.14 eV.

3. CO adsorption on $\frac{1}{2}$ ML Ni in subsurface sites of Cu(110)

First we have checked the most favorable adsorption sites for CO on the subsurface Ni atoms by using a (1×1) unit cell. It turned out that the on-top site is favored ($E_{\text{ads}} = -0.67$ eV) versus the short-bridge site ($E_{\text{ads}} = -0.55$ eV). This has been taken into account for the following calculations where again a (2×2) unit cell with 1–4 CO molecules was used. The results are compiled in Table V and Figs. 10(a)–10(d). We start for the 1 ML situation with an initial configuration of CO molecules located on each Ni atom in the fourfold hollow sites and with CO molecules located at the adjacent Cu rows either in short-bridge or on-top sites. It turns out that all the molecules become slightly tilted but no significant rearrangement of the molecules takes place after relaxation [Fig. 10(a)]. It is worth mentioning that in this case also a non-negligible tilting in the y direction (along the $[1-10]$ direction) shows up. Removing successively the CO molecules, first from the Cu sites and subsequently from the Ni sites, yields adsorption energies of about 0.5 eV for the first two molecules, 0.72 eV for the third, and 1.11 eV for the fourth molecule. In all cases, but, in particular, for the $\frac{1}{2}$ ML situation, a rather unusual tilting of the CO molecules in the x direction can be observed, where the C atoms tend to move closer to the threefold hollow sites of the (111) facets of the bimetallic (110) surface. This is shown in a side view in Fig. 10(c).

4. CO adsorption on a mixture of $\frac{1}{4}$ ML adsorbed and $\frac{1}{4}$ ML in-surface Ni atoms on Cu(110)

The previous calculations have shown that no good agreement can be obtained between the calculated adsorption en-

TABLE IV. Tilt angles and adsorption energies of CO on a 1:1 Ni/Cu(110) surface alloy as a function of CO coverage. Compare with Fig. 9.

Coverage (ML)	Tilt angle in the x direction ($^\circ$) n th molecule/C-O/Me-C			Adsorption energy (eV) /(n th molecule)
	First	Second	Third	
1	First	19	16	0.38 (first)
	Second	–18	–22	
	Third	–23	–18	
	Fourth	20	19	
0.75	Second	23	25	0.82(second)
	Third	–25	–19	
	Fourth	–7	–12	
0.50	Third	–21	–20	1.73 (third)
	Fourth	20	20	
0.25	Fourth	0	0	2.14 (fourth)

TABLE V. Tilt angles and adsorption energies of CO on Cu(110) with $\frac{1}{2}$ ML Ni in subsurface sites, as a function of coverage. Compare with Fig. 10.

Coverage (ML)		Tilt angle in the x direction ($^\circ$) n th molecule/C-O/Me-C		Adsorption energy (eV) /(n th molecule)
1	First	-10	-11	0.50 (first)
	Second	10	16	
	Third	13	-20	
	Fourth	-8	19	
0.75	Second	10	12	0.52(second)
	Third	0	-22	
	Fourth	-11	13	
0.50	Third	6	-22	0.72 (third)
	Fourth	-6	22	
0.25	Fourth	-8	10	1.11 (fourth)

ergies and the experimentally obtained desorption peaks. Therefore we have extended our calculations by taking into account a mixture of different nickel sites on the Cu(110) surface. A quite obvious arrangement would be that every second Ni atom from an adsorbed Ni row moves into an in-surface site. The relaxed configurations of CO adsorption sites for coverages ranging from 0.25 to 1 ML on such a bimetallic surface are shown in Fig. 11 and the tilt angles and adsorption energies are compiled in Table VI. Again, for coverages ≤ 0.5 ML the adsorption energies are about 1.9 eV, which is too large to explain the β peaks.

5. CO adsorption on a mixture of $\frac{1}{4}$ ML in-surface and $\frac{1}{4}$ ML subsurface Ni atoms on Cu(110)

Equivalent calculations have been carried out for a bimetallic surface consisting of $\frac{1}{4}$ ML of Ni atoms in surface sites

and $\frac{1}{4}$ ML of Ni atoms in adjacent subsurface sites. The results are compiled in Fig. 12 and Table VII. At a CO coverage of 1 ML, half of the CO molecules in the surface unit cell are adsorbed next to in-surface Ni atoms (fourth and third CO) with alternate tilting, $\frac{1}{4}$ are adsorbed on top of the subsurface nickel (second CO) and $\frac{1}{4}$ occupy on-top sites of Cu (first CO). The adsorption energy of the latter is only 0.45 eV. The removal of the weakly bound CO molecules does not influence the molecule configuration of the third and fourth CO but the second CO becomes slightly displaced. The removal of this molecule costs an energy of 0.93 eV. Finally, for the removal of the third CO molecule an energy of 1.1 eV and for the fourth CO an energy of 1.65 eV is needed. Apparently, these desorption energies coincide best with the experimentally obtained values for the β_1 - β_3 peaks. Again, we would like to emphasize that for this particular Ni configuration quite significant tilting of the CO molecules in the y direction takes place.

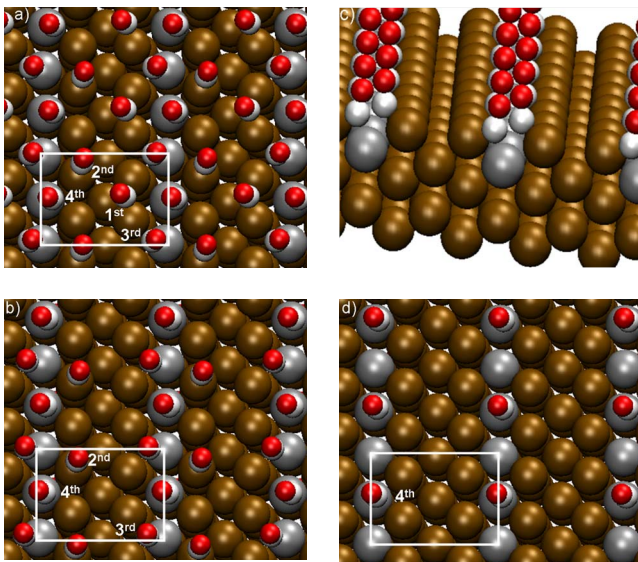


FIG. 10. (Color online) [(a)–(d)]: Relaxed CO molecule configuration on a Ni/Cu(110) bimetallic surface with $\frac{1}{2}$ ML nickel in subsurface sites, forming a (1×2) superstructure. (a) 1 ML CO, (b) 0.75 ML CO, (c) 0.5 ML CO, and (d) 0.25 ML CO.

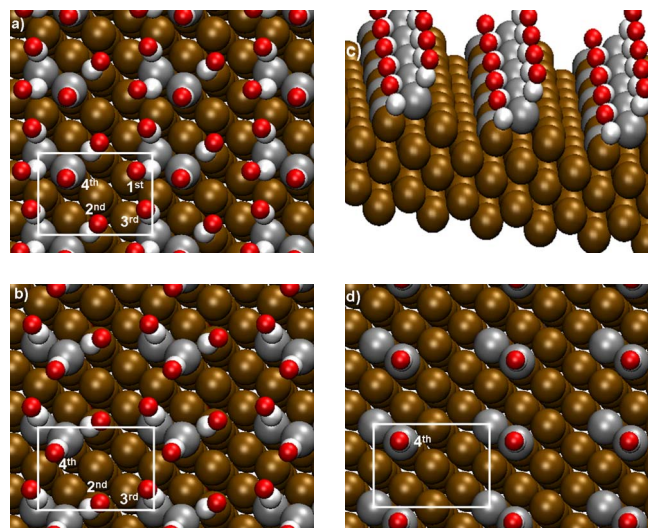


FIG. 11. (Color online) [(a)–(d)]: Relaxed CO molecule configuration on a Ni/Cu(110) bimetallic surface with $\frac{1}{4}$ ML adsorbed nickel and $\frac{1}{4}$ ML nickel in surface sites. (a) 1 ML CO, (b) 0.75 ML CO, (c) 0.5 ML CO, and (d) 0.25 ML CO.

TABLE VI. Tilt angles and adsorption energies of CO on a Ni/Cu(110) bimetallic surface [1/4 ML Ni adsorbed and $\frac{1}{4}$ ML Ni in surface sites on Cu(110)] as a function of CO coverage. Compare with Fig. 11.

Coverage (ML)		Tilt angle in the x direction ($^{\circ}$) n th molecule/C-O/Me-C		Adsorption energy (eV) /(n th molecule)
1	First	-42	-6	0.34 (first)
	Second	35	-5	
	Third	-9	0	
	Fourth	0	14	
0.75	Second	40	-6	0.94(second)
	Third	-15	5	
	Fourth	0	-11	
0.50	Third	-28	8	1.88 (third)
	Fourth	5	17	
0.25	Fourth	4	6	1.96 (fourth)

VI. DISCUSSION

The most intriguing result of this work is that the desorption temperature of CO on the bimetallic Ni/Cu(110) surface does not change continuously with increasing nickel concentration, by going from a clean Cu(110) surface (desorption peak temperature: 210 K) to a clean Ni(110) surface (desorption peak temperature: 420 K). Contrary, three distinct sharp desorption peaks additionally emerge at 250, 300, and 360 K. This suggests that the CO adsorption energies are determined by short-range geometrical arrangements rather than by long-range electronic effects.

The new adsorption peaks are more pronounced when Ni is produced on the surface by decomposition of Ni(CO)₄ than by physical vapor deposition of nickel. However, when Ni is evaporated onto a CO precovered Cu(110) surface or in a CO atmosphere, then the desorption spectra are very similar to that obtained after nickel carbonyl decomposition. Thus we believe that in both cases, after nickel carbonyl decomposition and after CO adsorption on the Ni evaporated surface, the CO desorption peaks are of the same physical origin. In particular, we do not believe that in the case of

nickel carbonyl exposure the β desorption peaks stem from direct decomposition of nickel subcarbonyls. On the other hand, the desorption features depend on the surface temperature during Ni evaporation. This hints to a very delicate influence of the local atomic arrangement at the bimetallic surface on the adsorbate and to an interplay between the CO adsorbate and the surface atoms. It is known that nickel atoms adsorbed on a copper surface are metastable at temperatures below 200 K.³⁴ With increasing temperature the atoms start to penetrate the surface and finally they become dissolved in the copper bulk. Unfortunately, this rearrangement of the nickel atoms might proceed in the same temperature range as CO desorption takes place.

In order to get insight into the thermodynamically stable phases of the CO/Ni/Cu(110) systems we calculated the total slab energies for various scenarios. In Fig. 13 the total energies of a five-layer copper slab, including two Ni atoms in various positions and different amounts of adsorbed CO are compiled. The arrangements of the Ni atoms correspond to the scenarios as depicted in Figs. 8–12: (*ad+ad*): both Ni atoms are adsorbed, (*ad+sa*): one Ni atom adsorbed and one Ni atom forming a surface alloy, (*sa+sa*): both Ni atoms are

TABLE VII. Tilt angles and adsorption energies of CO on a Ni/Cu(110) bimetallic surface [1/4 ML Ni in surface sites and $\frac{1}{4}$ ML in subsurface sites on Cu(110)] as a function of CO coverage. Compare with Fig. 12.

Coverage (ML)		Tilt angle in the x direction ($^{\circ}$) n th molecule/C-O/Me-C		Adsorption energy (eV) /(n th molecule)
1	First	0	-7	0.45 (first)
	Second	0	11	
	Third	15	14	
	Fourth	-14	-18	
0.75	Second	0	17	0.93(second)
	Third	19	20	
	Fourth	-18	-16	
0.50	Third	22	20	1.10 (third)
	Fourth	-23	-22	
0.25	Fourth	-5	-5	1.65 (fourth)

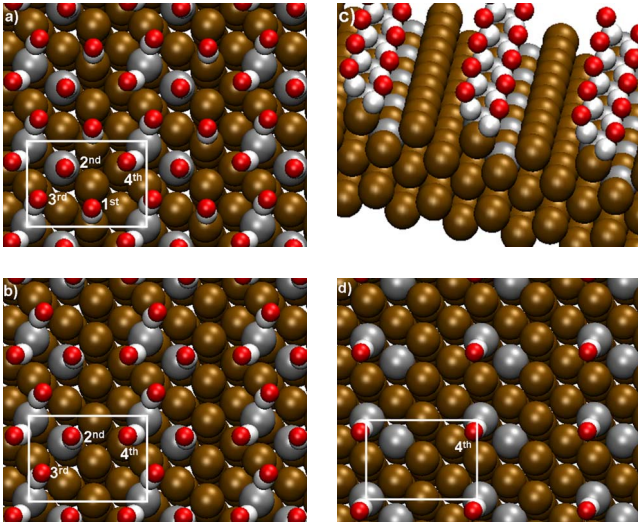


FIG. 12. (Color online) [(a)–(d)]: Relaxed CO molecule configuration on a Ni/Cu(110) bimetallic surface with $\frac{1}{4}$ ML nickel in surface sites and $\frac{1}{4}$ ML in subsurface sites. (a) 1 ML CO, (b) 0.75 ML CO, (c) 0.5 ML CO, and (d) 0.25 ML CO.

in in-surface sites, ($sa+ss$): one Ni atom in surface site and one Ni atom in subsurface site, and ($ss+ss$): both Ni atoms are located in subsurface sites. ($ss+ss1$) and ($ss1+ss1$): Ni atoms located in deeper layers. The plotted energies correspond to the total energies of a five-layer slab with a (2×2) unit cell, including two Ni atoms in the various positions, i.e., 20 atoms in total. In order to have comparable energies for the individual scenarios, in the ($ad+ad$) case the bulk energy of two Cu atoms and in the case of ($ad+sa$) the bulk energy of one Cu atom had to be subtracted. Furthermore, 1–4 CO molecules were placed on the bimetallic surface as shown in Figs. 8–12.

The calculations show that on the clean bimetallic surface the Ni atoms tend to move into subsurface states where a local energy minimum exists. However, when CO molecules are adsorbed on the surface, going from $\frac{1}{4}$ ML CO to 1 ML CO, it is energetically more favorable when the Ni atoms remain in the adsorbed configuration. This is exactly what we have also observed experimentally. One could now argue that the individual β desorption peaks are actually the result of the complex interplay between the Ni stabilization by CO and the Ni dissolution after partial CO desorption. Although we cannot fully exclude this scenario, the experimental data, however, indicate that in the temperature range between 200 and 500 K the arrangement of the Ni atoms in the surface unit cell is not changed considerably. This has been checked by various temperature-dependent Ni preparations at the copper surface and the corresponding influence on the CO desorption. In particular, this can be inferred from the simultaneous increase in the β desorption peaks as a function of $\text{Ni}(\text{CO})_4$ decomposition (Fig. 2), as well as from the common decrease in these peaks as a function the Ni preparation temperature (Fig. 4). This indicates that islands of the particular bimetallic surface exist which grow during Ni decomposition or evaporation and shrink during sample heating, respectively. The CO desorption spectra are then a mixture of desorption from these bimetallic islands with a largely stable

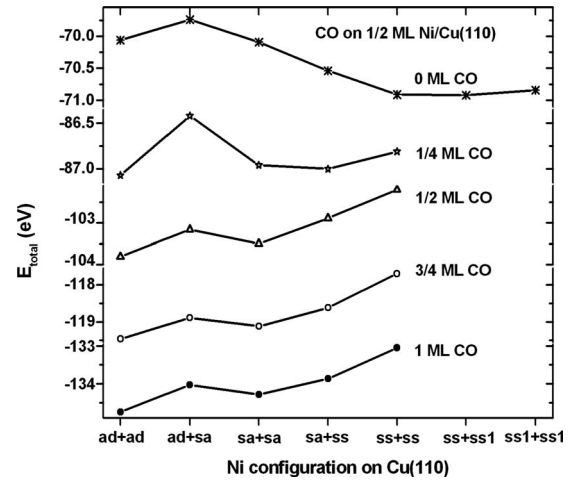


FIG. 13. Total energies of five-layer copper slabs with (2×2) unit cells, including two Ni atoms in various positions and different amounts of adsorbed CO. The arrangements of the nickel atoms correspond to the scenarios as depicted in Figs. 8–12. It is evident that without CO (upper curve) the Ni atoms tend to go into subsurface layers, whereas with adsorbed CO (lower curves) the Ni atoms tend to stay on the surface. For details see the text.

Ni/Cu arrangement and the clean parts of the surface.

Thus, the aim of this work was to find a correlation between the new, distinct CO desorption peaks and the specific adsorption sites on the bimetallic Ni/Cu(110) surface. As a starting point and for comparison with the experiment the adsorption energies for CO on the clean Cu(110) and Ni(110) surfaces were calculated. The obtained values of 0.8 eV for Cu(110) and 1.8 eV for Ni(110) are larger than the experimentally determined values due to the well-known problems of DFT calculations for CO adsorption energies.²² CO desorbs from Cu(110) with a first-order reaction kinetics at around 210 K when heated with 2 K/s ($\Theta < 0.5$ ML). A desorption energy of $0.6 \text{ eV} \pm 10\%$ and a pre-exponential factor ranging from 1×10^{13} to $1 \times 10^{14} \text{ s}^{-1}$ was reported in the literature.^{11,12,26} For CO desorption from Ni(110), which takes place at around 420 K for low coverages and a heating rate of 2 K/s, desorption energies between 1.2 (Ref. 30) and 1.4 eV (Ref. 13) were reported with pre-exponential factors ranging from 1×10^{13} to $8 \times 10^{15} \text{ s}^{-1}$. On the average, the correlation between the desorption peak maxima T_m and the desorption energies E_{des} can be quite well described by the Redhead formula for first-order desorption³⁵

$$E_{des} \approx kT_m \left[\ln \left(\frac{\nu T_m}{\beta} \right) - 3.64 \right]. \quad (2)$$

We use this formula to determine the desorption energies for the individual desorption peaks from the peak maxima T_m observed in our studies: α_1 (Cu): 210 K, β_1 : 250 K, β_2 : 300 K, and β_3 : 360 K and α (Ni): 420 K, assuming a similar desorption kinetics for all desorption peaks. Thus, we take an average pre-exponential factor of $1 \times 10^{14} \text{ s}^{-1}$ for the calculations. The heating rate is $\beta = 2 \text{ K/s}$. This yields $E_{des}[\alpha_1(\text{Cu})] = 0.61 \text{ eV}$, $E_{des}(\beta_1) = 0.73 \text{ eV}$, $E_{des}(\beta_2) = 0.88 \text{ eV}$, $E_{des}(\beta_3) = 1.06 \text{ eV}$, and $E_{des}[\alpha(\text{Ni})] = 1.24 \text{ eV}$.

(An error of the pre-exponential factor by one order of magnitude effects the calculated desorption energy only by about 0.06 eV.) A comparison of the calculated and experimentally obtained desorption energies for the clean surfaces yields that the calculated values are too large by a factor of about 1.4. We use this factor to determine the expected calculated values for the β_1 - β_3 peaks and obtain $E_{des}^{calc}(\beta_1) = 1.0 \pm 0.1$ eV, $E_{des}^{calc}(\beta_2) = 1.2 \pm 0.1$ eV, and $E_{des}^{calc}(\beta_3) = 1.5 \pm 0.1$ eV.

Let us next analyze the calculated adsorption energies obtained for CO on the various bimetallic surfaces. In principle, determining the most likely scenario underlying the thermal desorption (TD) spectra would require the evaluation of the barriers for possible exchange processes in the substrate and an adequate modeling of these processes within a kinetic treatment. Such an extensive modeling is beyond the scope of the present study. Instead, we sketch the most likely processes based on the energetics of the structure and the comparison of the corresponding calculated CO adsorption energies with the observed desorption peaks. In case of nickel adsorbed on Cu(110), for a half monolayer coverage in the form of a (1×2) superstructure as well as for a full nickel monolayer (calculations not shown), the highest adsorption energy for CO ($\Theta = 0.25$ ML) is 2.2 eV. This is even larger than the calculated value for CO adsorption on the pure Ni(110) sample (1.8 eV). At first glance this seems to be a surprising result. However, it has been shown recently that the deposition of a more reactive metal (e.g., Ni) onto a less reactive metal substrate (e.g., Cu) makes the overlayer even more reactive with respect to CO adsorption.⁷ This is explained by the weaker coupling of the reactive overlayer to the inert substrate, resulting in a stronger bonding to the adsorbate. Thus, the calculated desorption energies for the β_1 - β_3 states cannot be correlated with CO bonding to adsorbed nickel on the Cu(110) surface.

The calculated adsorption energies for CO on a 1:1 Ni-Cu surface alloy are similar to that on the nickel adsorbed layer. Again, the adsorption energies of 1.73 eV (0.5 ML) and 2.07 eV (0.25 ML) are too high to explain the β peaks. On the other hand, the calculation for CO adsorption on a subsurface Ni layer [$1/2$ ML in (1×2) configuration] yields too small values for the adsorption energies. In this case for the most strongly bound CO molecules (0.25 ML) an adsorption energy of just 1.0 eV is calculated (see Table V).

Reasonable adsorption energies could only be obtained from DFT calculations by assuming a mixture of adsorbed, in-surface and subsurface Ni atoms. In particular, the arrangement of $1/4$ ML Ni in surface sites and $1/4$ ML in subsurface sites, as shown in Fig. 12, yields a set of adsorption energies which are close to the expected ones, as summarized in Table VII. The smallest adsorption energy of 0.46 eV for the first molecule in the surface unit cell, which occupies an on-top Cu site is similar to that of the long bridge adsorbed CO on a clean Cu(10) surface (cf. Table I). This adsorption energy can be correlated with the α_2 peak (175 K) in the desorption spectrum (Fig. 3). It also explains why this peak does not decrease very much with increasing Ni coverage on the surface.

The calculated adsorption energy for the second CO molecule in the surface unit cell (on-top adsorption at subsurface

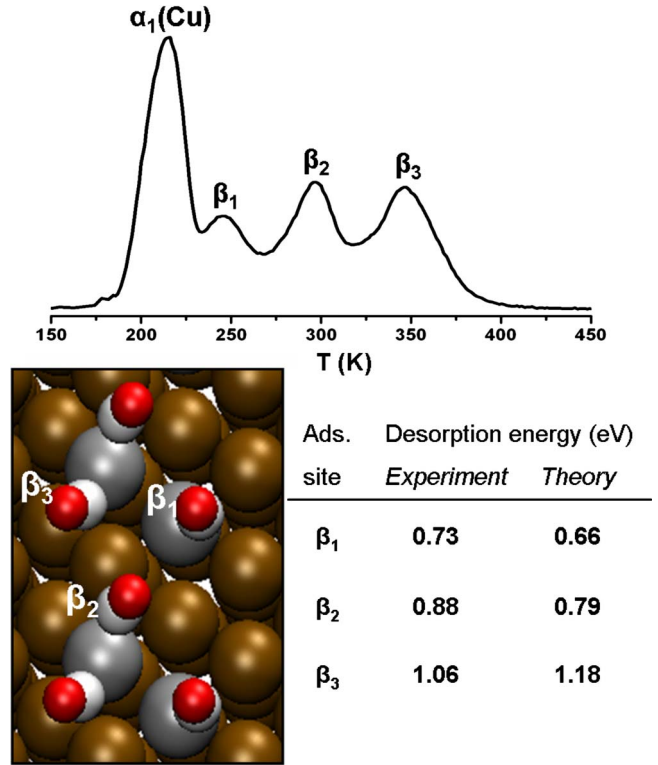


FIG. 14. (Color online) Compilation of the experimental CO desorption peaks and the associated adsorption sites on the Ni-Cu(110) bimetallic surface, as obtained by DFT calculations. The experimental and the theoretical values for the CO desorption energies of the β states are also inserted. Note that the theoretical values are those from Table VII, divided by the factor of 1.4, due to the overestimation of the CO binding energy, as described in the text.

nickel) is 0.93 eV. This peak can be correlated with the β_1 desorption peak with an expected desorption energy of 1.0 ± 0.1 eV. The calculated adsorption energies for the further CO molecules in the surface unit cell are 1.1 eV for the third and 1.65 eV for the fourth CO molecule, respectively. They can be correlated quite well with the β_2 peak (expected value: 1.2 ± 0.1 eV) and the β_3 peak (expected value: 1.5 ± 0.1 eV). It seems that only these special dimers, consisting of adjacent in-surface and subsurface nickel atoms, yield adsorption energies which can be reconciled with the experimental results. These final results are summarized in Fig. 14, where a typical CO desorption spectrum is shown and the calculated arrangement of the CO molecules on this special bimetallic surface. In addition, the experimental desorption energies of β_1 - β_3 and the corresponding calculated adsorption energies are inserted. Please note that in this case the calculated values have been divided by the above-described factor of 1.4, to account for the known overestimation of the CO adsorption energies in DFT calculations.

Calculations for increased nickel coverage (not shown), in adsorbed, in-surface and/or subsurface sites always lead to increased adsorption energies for small CO coverage. This is in accord with the experimental data for CO adsorption on the bimetallic surface with increased nickel coverage, which shows a continuous shift of the β_3 state into the α (Ni) state (Fig. 3). However, we never observed a CO desorption peak

temperature on the bimetallic surface which was larger than that on the clean Ni surface. This implies that at temperatures above 400 K no stable thin nickel layer ($\Theta \leq 1$ ML) can be preserved on the Cu(110) surface. On the other hand, thicker nickel films ($\Theta > 4$ ML) remain adsorbed at least during short heating up to 500 K (above the CO desorption temperature on clean nickel).

VII. SUMMARY AND CONCLUSIONS

The adsorption behavior of CO on the bimetallic Ni/Cu(110) surface has been studied experimentally by thermal-desorption spectroscopy, including Auger electron spectroscopy and low-energy electron diffraction, and theoretically by DFT calculations. The bimetallic surface was produced either by evaporation of nickel or by decomposition of Ni(CO)₄ on Cu(110). With both methods similar bimetallic surfaces could be obtained. Adsorption of CO on such a bimetallic surface yields three new adsorption states with adsorption energies between that on clean Cu(110) and clean Ni(110). The desorption peak maxima for CO on clean Cu(110) are located at 210 K and on clean Ni(110) at 420 K. The new desorption peaks from the bimetallic surface, labeled as β_1 - β_3 , can be observed at 250, 300, and 360 K,

respectively. These new states are most pronounced when $\frac{1}{2}$ monolayer of nickel is present on the Cu(110) surface. This result shows that CO adsorption is determined by local (geometric) effects rather than by long-range (electronic) effects.

A great number of DFT calculations, using the VASP code, were performed to identify the most probable Ni/Cu atomic arrangement at the bimetallic surface to reconcile with the experimental results. It turned out that CO adsorption on nickel dimers consisting of in-surface and adjacent subsurface atoms give the best agreement with the observed experimental data.

These results should contribute to a better understanding of tailoring catalytic processes with the help of bimetallic catalysts. Both the reactivity and selectivity of a catalyst can be influenced in this way because generally a specific arrangement of the surface atoms (ensemble) is needed to run a catalytic reaction and appropriate adsorption energies for the reactants have to be available.

ACKNOWLEDGMENT

This research project has been supported by the Austrian Science Fund, FWF under Project No. P20026.

*Corresponding author. FAX: +43 316 873 8466; a.winkler@tugraz.at

- ¹W. H. M. Sachtler, *Faraday Discuss. Chem. Soc.* **72**, 7 (1981).
- ²C. T. Campbell, *Annu. Rev. Phys. Chem.* **41**, 775 (1990).
- ³D. W. Goodman, *Surf. Sci.* **299-300**, 837 (1994).
- ⁴J. A. Rodriguez, *Surf. Sci. Rep.* **24**, 223 (1996).
- ⁵V. Ponec, *Appl. Catal., A* **222**, 31 (2001).
- ⁶J. G. Chen, C. A. Menning, and M. B. Zellner, *Surf. Sci. Rep.* **63**, 201 (2008).
- ⁷A. Groß, *Top. Catal.* **37**, 29 (2006).
- ⁸S. Sakong, C. Mosch, and A. Groß, *Phys. Chem. Chem. Phys.* **9**, 2216 (2007).
- ⁹A. Groß, *J. Phys.: Condens. Matter* **21**, 084205 (2009).
- ¹⁰P. Sabatier, *Ber. Deutsch. Chem. Gesellschaft* **44**, 1984 (1911).
- ¹¹C. Harendt, J. Goschnick, and W. Hirschwald, *Surf. Sci.* **152-153**, 453 (1985).
- ¹²M. Christiansen, E. V. Thomsen, and J. Onsgaard, *Surf. Sci.* **261**, 179 (1992).
- ¹³J. L. Falconer and R. J. Madix, *Surf. Sci.* **48**, 393 (1975).
- ¹⁴R. J. Behm, G. Ertl, and V. Penka, *Surf. Sci.* **160**, 387 (1985).
- ¹⁵K. Y. Yu, D. T. Ling, and W. E. Spicer, *Solid State Commun.* **20**, 751 (1976).
- ¹⁶N. J. Castellani, *Int. J. Quantum Chem.* **41**, 599 (1992).
- ¹⁷D. Shriver, P. Atkins, and C. Lanford, *Inorganic Chemistry* (W.H. Freeman, New York, 1990).
- ¹⁸K. Lascelles and L. V. Renny, *Surf. Sci.* **125**, L67 (1983).
- ¹⁹G. Kresse and J. Furthmüller, *Phys. Rev. B* **54**, 11169 (1996).
- ²⁰J. P. Perdew, K. Burke, and M. Ernzerhof, *Phys. Rev. Lett.* **77**,

3865 (1996).

- ²¹G. Kresse and D. Joubert, *Phys. Rev. B* **59**, 1758 (1999).
- ²²G. Kresse, A. Gil, and P. Sautet, *Phys. Rev. B* **68**, 073401 (2003).
- ²³P. J. Feibelman, B. Hammer, J. K. Norskov, F. Wagner, M. Scheffler, R. Stumpf, R. Watwe, and J. Dumesic, *J. Phys. Chem. B* **105**, 4018 (2001).
- ²⁴F. Mehmood, A. Kara, T. S. Rahman, and K. P. Bohnen, *Phys. Rev. B* **74**, 155439 (2006).
- ²⁵S. Y. Liem and J. H. R. Clarke, *J. Chem. Phys.* **121**, 4339 (2004).
- ²⁶J. Ahner, D. Mocuta, R. D. Ramsier, and J. T. Yates, Jr., *J. Chem. Phys.* **105**, 6553 (1996).
- ²⁷S. Vollmer, G. Witte, and C. Wöll, *Catal. Lett.* **77**, 97 (2001).
- ²⁸K. Horn, M. Hussain, and J. Pritchard, *Surf. Sci.* **63**, 244 (1977).
- ²⁹P. Hofmann, K.-M. Schindler, S. Bao, V. Fritzsche, A. M. Bradshaw, and D. P. Woodruff, *Surf. Sci.* **337**, 169 (1995).
- ³⁰M. D. Alvey, M. J. Dresser, and J. T. Yates, Jr., *Surf. Sci.* **165**, 447 (1986).
- ³¹B. A. Gurney and W. Ho, *J. Vac. Sci. Technol. A* **3**, 1541 (1985).
- ³²S. Yang, M. Yu, G. Meigs, X. H. Feng, and E. Garfunkel, *Surf. Sci.* **205**, L777 (1988).
- ³³Y. Tzeng, H. Wu, K. Shiang, and T. Tsong, *Phys. Rev. B* **48**, 5549 (1993).
- ³⁴L. V. Pourovskii, N. V. Skorodumova, Yu. Kh. Vekilov, B. Johansson, and I. A. Abrikosov, *Surf. Sci.* **439**, 111 (1999).
- ³⁵P. A. Redhead, *Vacuum* **12**, 203 (1962).